In-situ catalytic conversion of tar using rice husk char-supported nickel-iron catalysts for biomass pyrolysis/gasification

Yafei Shen [a,*], Peitao Zhao [a,b], Qinfu Shao [a,c], Dachao Ma [a], Fumitake Takahashi [a], Kunio Yoshikawa [a]

[a] Department of Environmental Science and Technology, Interdisciplinary Graduate School of Science and Engineering, Tokyo Institute of Technology, G5-8, 4259 Nagatsuta, Midori-ku, Yokohama 226-8502, Japan
[b] Key Laboratory of Energy Thermal Conversion and Control of Ministry of Education, School of Energy and Environment, Southeast University, Nanjing 210096, PR China
[c] Laboratory of Waste-coexistence Engineering, Department of Environmental Engineering, Osaka Institute of Technology, Asahi-ku, Osaka 533-8585, Japan

ARTICLE INFO

ABSTRACT

This paper aims to propose an effective tar conversion approach during biomass pyrolysis via *in-situ* dry reforming over rice husk (RH) char and char-supported Ni-Fe catalysts. Utilizing high pyrolysis temperature, tar from biomass pyrolysis could be removed effectively in the gasifier by mixing with the char-supported catalysts, simplifying the follow-up tar removal process. Under the optimized conditions, the conversion efficiencies of condensable tar can reach about 92.3% and 93% using Ni-Fe char (without calcination) and Ni char (with calcination), respectively. It is noteworthy that the condensable tar could be catalytically transformed into the non-condensable tar or small molecule gases resulting in the heating value increase of gaseous products to benefit of the power generation systems. Compared with the other catalysts preparation methods, Ni–Fe char exhibited more advantages of convenient and energy-saving. In the presence of catalysts, the concentration of CO_2 (vol.%) was reduced slightly, while the CO concentration (vol.%) increased greatly because of dry reforming. Due to carbon loss, parts of RH char-supported catalysts (C-SiO_2 catalysts) could be converted into SiO_2-based catalysts because of high-content amorphous nano-sized SiO_2 in RH char. In addition, partial metal oxides or ions via carbon (i.e., biochar) and gas (i.e., H_2, CO) *in-situ* reduction were transformed into metallic states contributing to the enhancement of tar conversion. Therefore, RH char plays two significant roles during the process of biomass pyrolysis. On one hand, it works as an intermediate reductant to reduce the metal oxides and CO_2; on the other hand, it can be considered as an adsorptive-support to adsorb metal ions and tar. After that, the char-supported catalysts could be used for tar conversion. In particular, since the metal catalysts still remain in the solid residues, the pyrolysis char could be regenerated via thermal regeneration using waste heat or gasified into syngas directly.

© 2014 Elsevier B.V. All rights reserved.

1. Introduction

Biomass pyrolysis/gasification is considered as one of the most promising technologies for production of sustainable fuels that can be used for power generation systems or syngas applications. Gasification of biomass has several environmental advantages over fossil fuels, namely lower emission of CO_2 and other flue gases such as H_2S, SO_2, NO_x [1–4]. Biomass gasification is a process in which biomass undergoes incomplete combustion to produce a gas product called syngas that consists mainly of H_2, CO, CH_4, CO_2, and N_2 (if air is used in combustion) in various proportions. Biomass gasification has many advantages over direct combustion. It converts low-value feedstocks to high quality combustible gases, which can be not only directly burned or used for electricity generation but also turned into liquid transportation fuels [5].

Processes occurring during biomass gasification are illustrated in Fig. 1A, the main processes are distinguished: drying and devolatilization, volatile and char combustion, and gasification and tar reforming with steam and CO_2. These processes can be identified in certain spatial regions in fixed bed gasifiers [6]. As shown in Fig. 1B, during transient heating of the particle, temperature increases locally, leading first to the evaporation of moisture (drying stage) and then to the progressive release of pyrolytic volatiles (primary pyrolysis stage). The primary volatiles are produced from

* Corresponding author. Tel.: +81 45 924 5507; fax: +81 45 924 5518.
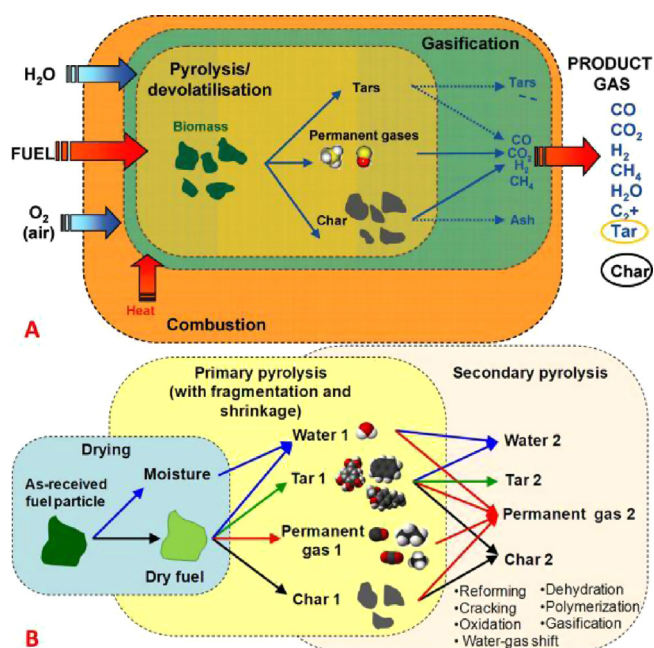 *E-mail address:* yafeisjtu@gmail.com (Y. Shen).

Fig. 1. (A) Main processes during biomass conversion in a gasifier: drying and devolatilization, volatile and char combustion, and gasification and tar reforming with steam and CO_2 [10]. (B) Thermal degradation of a solid biomass particle under inert atmosphere: drying, primary pyrolysis and secondary pyrolysis [9].

the thermal scission of chemical bonds in the individual constituents of biomass, which are cellulose, hemicellulose, lignin and extractives, and comprise permanent gas species (e.g., CO_2, CO, CH_4) and condensable species at ambient conditions (several organic compounds and water). Although each of the biomass constituents decompose at faster rates in different temperature ranges, the overall primary pyrolysis stage is complete at relatively low temperatures (<500 °C), yielding a carbon-rich non-volatile solid that is called char or charcoal. The produced char also contain a significant part of the mineral matter originally present in the parent fuel. Nevertheless, if the fuel is converted at higher temperatures some of the primary volatiles released inside the particle can further participate in a variety of secondary reactions to form product "2". Serial and parallel reactions can take place, occurring either heterogeneously or homogeneously, such as cracking, reforming, dehydration, and so on [7–9].

organics (i.e., polycyclic aromatic hydrocarbons) referred to as "tar" are produced along with syngas during biomass gasification and their contents vary from 0.5 to 100 g/m³ depending on the type and design of gasifier, feedstock types, and operating conditions [10]. Tar is a generic term comprising all organic compounds present in syngas except for gaseous hydrocarbons. Tars can condense to more complex structures in pipes, filters, or heat exchangers of downstream equipment and processes, which may cause mechanical breakdown of the entire system. Tars may also deactivate catalysts in the refining process. Tar removal by efficient adsorption and reforming to syngas should be important and indispensable to commercialize this technology for applications in power generation and synthetic fuel production [11]. It is essential to reduce the level of tars to enable widespread utilization of syngas. Several approaches for tar elimination, such as physical treatment [12–14], thermal cracking [15], plasma-assisted cracking [16], and catalytic reforming [17–21], have been widely reported. Among these, catalytic reforming is considered the most promising in large-scale applications because of its fast reaction rate and reliability [21] and its ability to increase the quantity of usable gases such as CO and H_2 in syngas.

Various types of catalysts such as calcined rocks [22], zeolites [23], iron ores [24], alkali metals [25], Ni-based catalysts [26,27], and noble metals [28–32] have been studied for their usefulness on tar removal in biomass gasification. For catalytic reactivity and economic reasons, Ni-based catalysts are considered the most promising for tar removal and syngas reforming [33–39]. Nickel catalysts are usually supported by metal oxides (e.g., Al_2O_3 and MgO) or natural materials (e.g., dolomite, olivine, activated charcoal) [40–45]. These supports are relatively expensive, and the catalyst preparation steps are time and energy consuming; these factors limit extensive application of Ni-based catalysts. As a promising alternative, chars have been reported to be an inexpensive catalyst with fair performance in tar removal [46–49] and also an excellent adsorbent [50]. The char-supported catalysts would have low costs and be simply gasified to recover the energy of the char without the need of expensive regeneration after deactivation. However, the disadvantages of biomass char are consumption because of gasification reactions and unfixed properties depending on biomass type and process conditions.

Recently, Wang et al. [51] investigated char and char-supported nickel catalysts for secondary syngas cleanup and conditioning. In this study, Ni-based catalysts were made by mechanically mixing NiO and char particles at various ratios. The Ni/coal-char and Ni/wood-char catalysts removed more than 97% of tars in syngas at 800 °C reforming temperature, 15% NiO loading, and 0.3 s gas residence time. Meanwhile, iron-based catalyst and additive Fe have attracted more attention of researchers. Nemanova et al. [52] reported the use of Fe based catalysts and the effect of iron-based granules on biomass tar decomposition. The use of these Fe based catalysts resulted in tar reduction. Liu et al. [53] studied the effect of different additives (Fe, Mg, Mn, Ce) on catalytic cracking of biomass tar over Ni_6/palygorskite. The result also demonstrated Fe played a better role in improving the reactivity of Ni_6/palygorskite.

Fe-based catalysts [54] are much cheaper, abundant and environmental friendly than Ni-based or other metal catalysts. Moreover, iron oxides possess various physicochemical properties, e.g., Fe_2O_3 (oxidation), Fe_3O_4 (magnetism), possibly enhancing the catalytic activity or decreasing the coking deposition. In the previous work, bimetallic catalysts, such as Fe–Co, Ni–Co alloy particles supported in Al_2O_3, were benefit for steam reforming of tars compared with Fe/Al_2O_3 and Co/Al_2O_3 [55,56]. However, the rice husk (RH) char-supported bimetallic Ni–Fe catalysts have been rarely reported for tar conversion. In this work, we proposed a novel biomass catalytic pyrolysis technology for *in-situ* tar conversion and upgrading using RH char and char-supported Ni or Fe catalysts.

2. Materials and methods

2.1. Biomass and char characterization

The biomass feedstock of RH was collected from Thailand. The ultimate and proximate analyses of RH and RH char shown in Table 1 were conducted by elemental analyzer (Vario MICRO Cube, Elementar, Germany) and DTG-50 (SHIMADZU, Nakagyo-ku, Kyoto, Japan), respectively. Besides, the chemical composition of rice husk ash (RHA) was analyzed by X-ray fluorescence "XRF" (SHIMADZU, Rayny EDX 700, Japan).

2.2. Catalysts preparation

RH char was prepared by slow pyrolysis at the temperature of 700 °C in the N_2 atmosphere. Three types of Ni char (Ni^{2+}: 0.2 mol/L), Fe char (Fe^{3+}: 0.2 mol/L) and Ni–Fe/char (Ni^{2+}: 0.1 mol/L,

Table 1
Proximate and ultimate analyses of RH and RH char.

Parameters	Ultimate analysis (wt.%, dry and ash free basis)					Proximate analysis (wt.%, dry basis)			BET surface area (m^2/g)
	C	H	O[a]	N	S	VM[c]	FC[d]	Ash	
RH	37.9	6.3	55.3	0.4	0.1	59.7	11.9	28.4	2.2
RH char	48.0	3.8	47.6	0.6	0	11.7	34.3	54.0	117.0[b]
RHA	–	–	–	–	–	5.4	7.8	86.8	65.4
					Chemical composition of RH ash (wt.%)				
SiO_2						94.64			
Al_2O_3						0.06			
Fe_2O_3						0.23			
CaO						1.88			
MgO						0.96			
Na_2O						0.39			
K_2O						0.58			
Zn (ppm)						18.20			
Mn (ppm)						52.24			
Cu (ppm)						32.17			
Cd (ppm)						0.48			

[a] Calculated by difference.
[b] 700 °C char, changed with pyrolysis temperature and method.
[c] VM: volatile matters.
[d] FC: fixed carbon.

Fe^{3+}: 0.1 mol/L) catalysts were prepared by the incipient wetness impregnation and calcination method using $Fe(NO_3)_3 \cdot 9H_2O$ (Wako Pure Chemical Industries, Ltd., Japan) and $Ni(NO_3)_2 \cdot 6H_2O$ (Wako Pure Chemical Industries, Ltd., Japan) as iron and nickel precursors with RH char, respectively. And Ni–Fe char (Ni^{2+}: 0.1 mol/L, Fe^{3+}: 0.1 mol/L) was prepared without calcination. The char adsorption ability of metal ions depend on the preparation methods and conditions, such as biomass char characteristics, temperature, metal ion types. The procedure of catalysts preparation was described briefly in Scheme 1. After impregnation and drying overnight at 105 °C, the char-supported catalysts were calcined in air at 600 °C for 1 h before storage and further use. The catalysts before and after reaction were characterized by X-ray diffraction "XRD" (Rigaku, XRD-DSC II, Japan), X-ray photoelectron spectroscopy "XPS" (Physical Electronics, USA), respectively.

2.3. Biomass pyrolysis and tar reforming system

The main experimental parameters of operating condition are shown in Table 2. The experimental apparatus includes a gas supplying system, an online syngas analysis system, a gas cleaning system and a two-stage pyrolysis facility, which was made from quartz, which is divided into three parts, an outer tube, a top cover with a feeding port and also a gas inlet and an inner tube. A sintered quartz porous plate was fixed in each tube to support the sample or char. The reactor was surrounded and heated in the temperature range of 600–900 °C by a two-zone electric furnace. The RH

Table 2
Main experimental parameters of operating conditions.

Condition	Parameter
Gasification style	Fast pyrolysis
Pyrolysis temperature (°C)	800
Biomass feedstock	Rice husk
Feedstock size (mm)	0.125–0.5
Sample weight (g)	~5
Carrier gas	N_2
Carrier gas flow rate (L/min)	1.0
Char particle size (mm)	Original size
Amount of used catalyst (g)	~5

feedstock was prepared by crushing and sieving with the particle size below 0.5 mm. The feedstock was dried in an oven at 105 °C overnight for moisture elimination before packing in the feeder. At first, the pyrolysis temperature was heated up to 800 °C. Then the nitrogen (N_2) was continuously leaded into the entire system before adding the feedstock, so it can insure that the fast pyrolysis reaction was carried out under the low-oxygen condition. When the feedstock mixed with char-supported catalyst was supplied into the pyrolyzer (first-zone), the volatile matters were released in the form of syngas and tar. Utilizing the waste heat in the first zone, parts of biomass tar could be *in-situ* reformed and upgraded simultaneously over the char-supported catalysts by thermochemical reactions in the first-zone. Residual tar was condensed and collected in the gas cleaning unit.
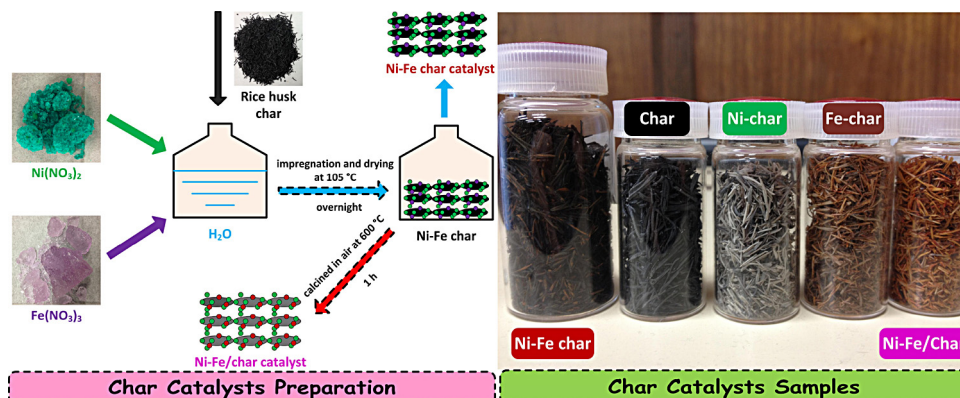
Scheme 1. Preparation of Ni–Fe/char catalysts via impregnation with or without calcination.
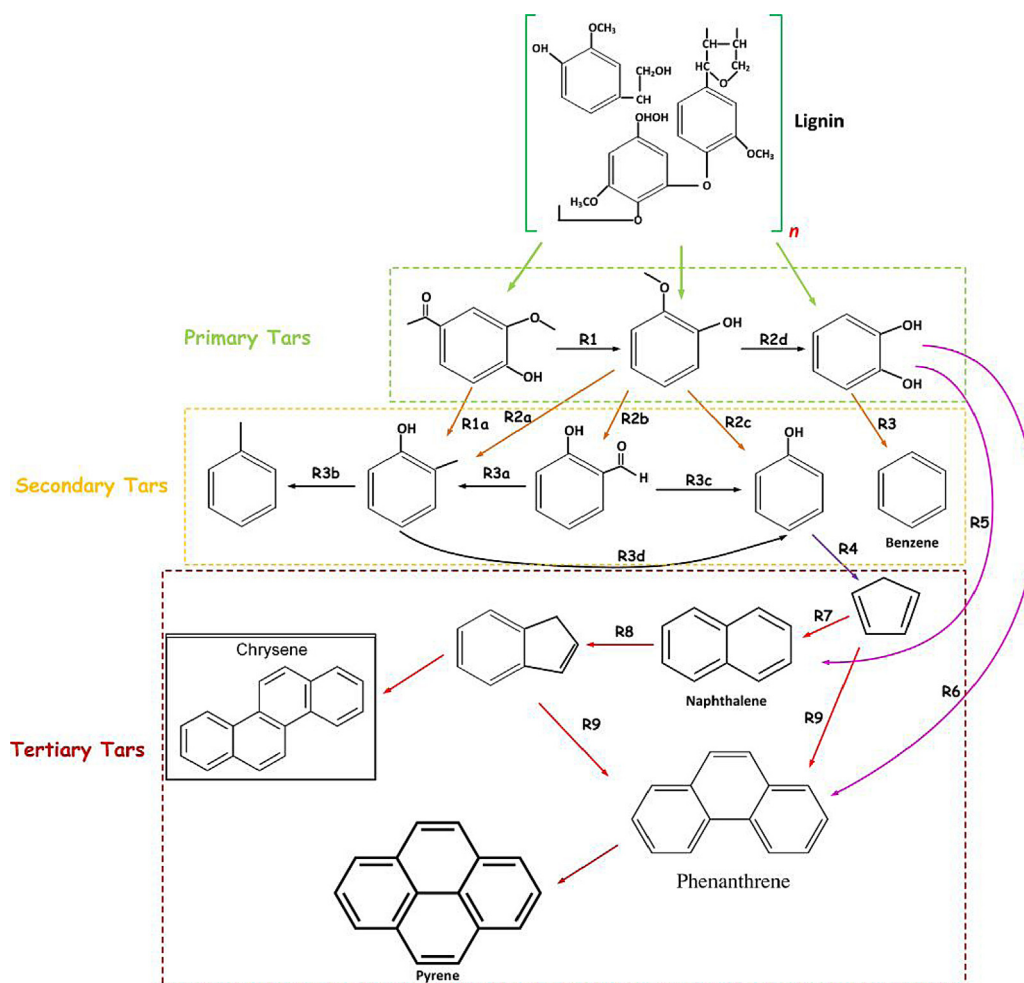
Scheme 2. Proposed mechanisms for primary, secondary, and tertiary tar formation.

2.4. Sampling and analysis

Biomass pyrolysis tar is a complex mixture, consisting of hundreds hydrocarbon compositions. Tars in this research were sampled and their amounts were analyzed by wet and dry methods, respectively. The wet method aims to analyze condensed high molecular weight tar droplets and determined by weight as gravimetric tar, called heavy tar. This wet method for heavy tar measurement has been modified along with the guideline for sampling and analysis of tar and particles in biomass syngas [57]. The syngas passed through a series of 3 impingers filled with 100 mL isopropanol under the ice bath, and tar was collected by both condensation and absorption. This impinger train was connected with filters, a gas flow meter, a manual control valve, and a suction pump, respectively. After sampling, all of isopropanol sampling solvent in each impinger were mixed together, filtrated and dried by a standard rotary evaporator in a water bath kept at 40 °C. Then, weigh the flask accurately and determine the amount of residue-heavy tar. Besides, the dry method aims to analyze the volatile tar aerosols (light tar) in the gas flow and fractionated by GC-FID (SHIMAZU, GC 14-B, Japan) [13,14]. The heavy tar components cannot be eluted through the GC columns. As for the gas compositions, the volume fraction of H_2, CH_4, CO, CO_2, and C2 hydrocarbons (i.e. C_2H_4, C_2H_6) were measured at the outlet by a micro gas chromatograph (VARIAN, Micro GC, CP4900) fitted with a thermal conductivity detector (TCD). Each trial was maintained for 30 min, and several repeat runs were carried out under the identical conditions to ensure the repeatability of the process.

3. Results and discussion

3.1. Characteristics of RH and RH char

Fig. 2 shows the scanning electron microscope (SEM) photographs of RH and RH char along with BET surface area are shown in Table 1. From these characterizations, it can be observed that RH char became a highly porous carbonaceous material after high-temperature pyrolysis, just like activated char. Therefore, it has suitable characteristics to be used as the catalyst support or adsorbent. Moreover, RH is very abrasive and wears conveying elements very quickly because of the high silica contents. RH has a typical globular structure in nature, of which its main components are in the lemma or palea form, tightly interlock with another (Fig. 2). The corrugate structural outer epidermis is highly ridged, containing papillae and hairs of varying sizes and well organized in a linear profile (linear ridges and furrows), while its ridges are punctuated with the prominent globular protrusions [58]. Whereas, the biomass are assembled around the stable Si–O carcass, concentrated in the protuberances and hairs (trichomes) on the outer and inner epidermis, adjacent to the rice kernel [59]. Many cavities having varying particle sizes were indicated distributing within the ash samples, evidenced of the interconnected porous net work and large internal specific surface area [60]. In our recent work [61], RH char obtained at the pyrolysis temperature of 700 °C can achieve a higher tar adsorption efficiency (more than 80%) contributed to its larger BET surface area ($\sim$17 m^2/g), which is much higher than some common-used natural materials such as dolomites (5–20 m^2/g) [62]. The
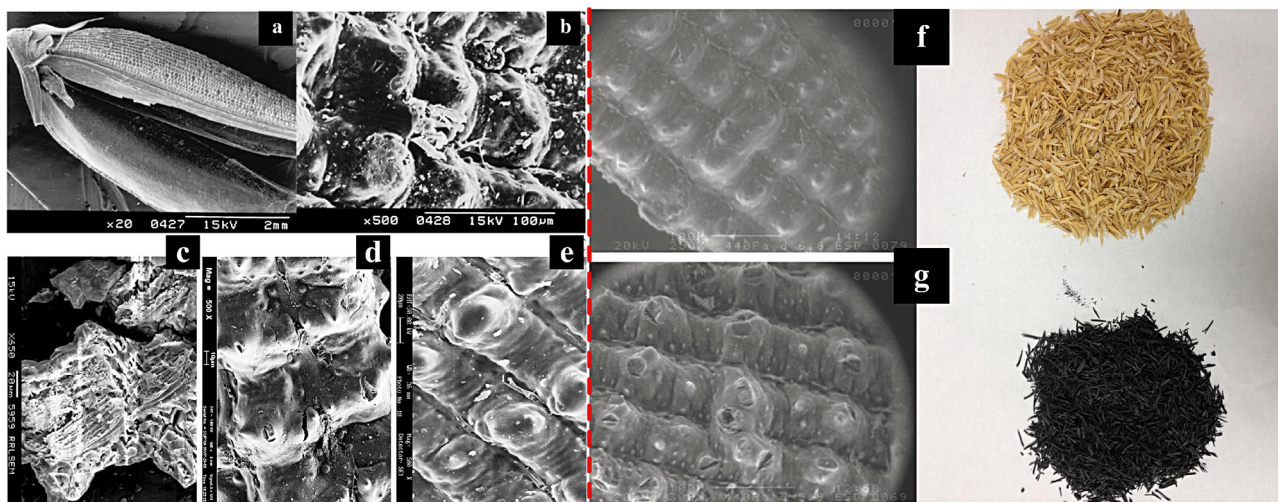
Fig. 2. SEM of fibrous RH (20×) (a), RH showing protuberance, outer epidermis and silica content (500×) (b), RH char (1000×) (c) and its morphological details (1000×) (d), (650×) (e); RH (f) and RH char (g) in this work.

large surface area of char is formed during the fast devolatilization of biomass at the primary pyrolysis stage.

Comparative nitrogen adsorption–desorption curves of the raw RH, RH char, RHA and γ-Al_2O_3 are shown in Fig. 3. According to the Brunauer–Deming–Deming–Teller classification, raw RH obeys type III adsorption isotherm, with no obvious hysteresis loop convex over the entire range, suggesting relatively low specific surface area, pore volume, weak forces and low adsorption capacity within the whole range of studied pressures. With the same classification, RH char and RHA are characterized by the type IV adsorption isotherm, resulting from the surface coverage of mesoporous walls followed by pore filling associated with various hysteresis loops. At relatively low P_i/P_0 values, the isotherms shape is similar to type II isotherm but at P_i/P_0 values above 0.4, pore condensation will be taking place, illustrating porous structure of the RH char and RHA. Hysteresis loops associated with capillary condensation in both samples are the narrow type H_1 hysteresis loop, with almost vertical and parallel branches (opened ended cylindrical channel with uniform size and shape), associated with delayed condensation and little percolation hold-up. It can indicate that carbonized RH char has better adsorption capacity for metal ions than RH and RHA. Thus, RH char can be modified and used as a high SiO_2-containing carbonaceous adsorbing material with high heat conductivity and thermal stability.
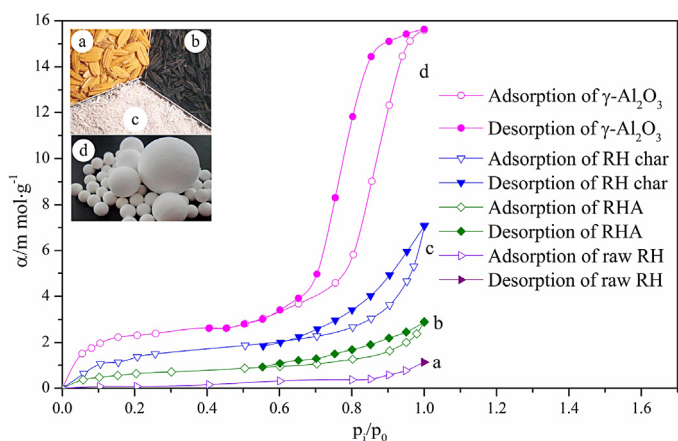
3.2. Catalysts characterization

Fig. 4 shows the thermogravimetric analysis (TGA) of char and char-supported catalysts under the air atmosphere. It can be observed that char-supported catalysts after calcination had high thermal stability. However, the weight of char and Ni–Fe char catalysts decreased with the increase of temperature under the air condition. When the heat temperature was above 400 °C, the weight of char decreased rapidly. After that, the weight became constant after the temperature up to 600 °C. It can conclude that char and Ni–Fe char are appropriate for tar conversion under the oxygen-free atmosphere to extend their service life. It is possible that most of carbon in RH char can easily react with oxygen and be oxidized into carbon oxides at high temperature. The high SiO_2-containing carbonaceous residue had high thermal stability and abrasive resistance. From the TGA curves of char and Ni–Fe char, it may also infer that the temperature range of 400–450 °C could be selected for *in-situ* thermal regeneration of the char-supported catalysts using the waste heat.

X-ray diffraction (Fig. 5) was used to identify the different crystalline phases and then to follow the structural modifications occurring before and after reforming tests. According to the PDF
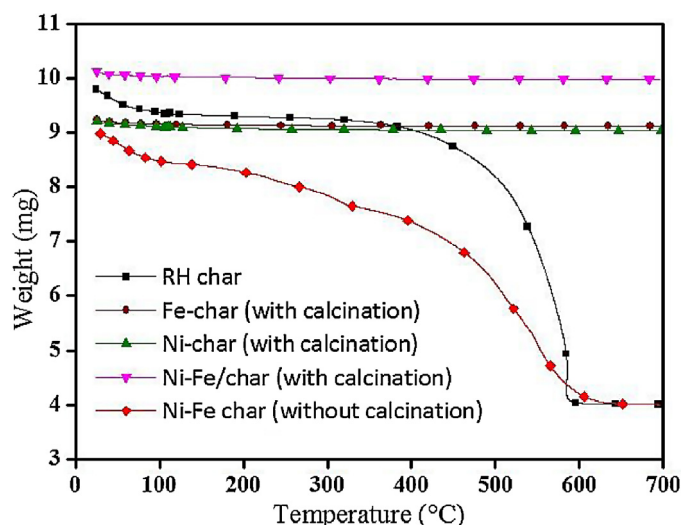

Fig. 3. Nitrogen adsorption–desorption isotherms at 77 K of grounded (a) raw RH, (b) RH char, (c) RHA and (d) γ-Al_2O_3.

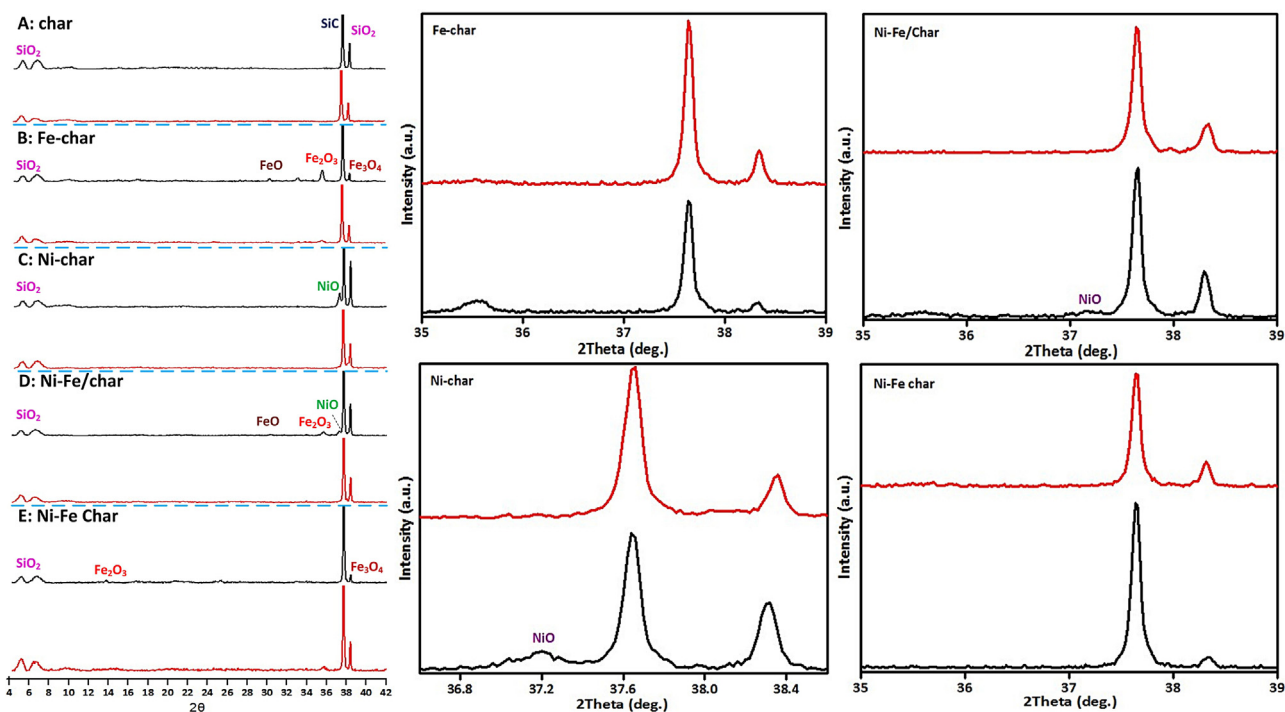**Fig. 4.** TGA of char and char-supported catalysts under the air atmosphere.

Fig. 5. XRD patterns of char-supportedcatalysts before (below line) and after reaction (up line). (For interpretation of the references to colour in this figure legend, the reader is referred to the web version of this article.)

card of standard diffraction datum, the RH char is a silica-based carbonaceous material in the forms of quartz, zeolites, MCM-41, MCM-48, etc. And SiO_2 (zeolite, MCM-41), SiC and Si/C crystalline matters could be obviously observed in Fig. 5A. The XRD patterns were normalized by the SiO_2 peaks at $2\theta = 5.0°$, $6.1°$, respectively. In addition, the strong peak at $2\theta = 37.6°$ was observed and identified as SiC or Si/C composites, showing a better crystalline structure. Although other minerals such as Al_2O_3, Fe_2O_3, CaO, MgO, existed in the RH char, their XRD diffraction peaks were too small to be identified in this research. In the Fe-char catalyst before reaction, the peaks at $2\theta = 30°$, $35.6°$, $38.5°$ were observed and identified as FeO, Fe_2O_3 and Fe_3O_4, respectively. It is possible that three iron oxides were loaded on the surface of SiO_2 resulting in the intensity of the SiO_2 peak decreased. After the processing, the peaks of three iron oxides disappeared. The reason may be attributed to the reductive and thermochemical reactions between carbon, tar and iron oxides at high temperature (Fig. 5B). Besides, the Ni-char and Ni–Fe/char catalysts were suffered as well (Fig. 5C, D). The peak of NiO can be clearly observed and identified at $2\theta = 37.2°$. Without calcination, crystalline Fe_2O_3 and Fe_3O_4 with low intensity could also be formed at lower temperature compared with NiO (Fig. 5E).

3.3. Tar conversion efficiency

Tar is a complex mixture of condensable or non-condensable hydrocarbons comprising single-ring to five-ring aromatic compounds along with other oxygen-containing hydrocarbons and complex polycyclic aromatic hydrocarbons (PAHs) produced during thermochemical conversion processes. The most frequent individual tar species studied experimentally and as model tars are acetol, acetic acid and guaiacols (primary tars), phenols, cresols and toluene (secondary tars), and naphthalene (tertiary tar). Biomass composition comprises lignin, cellulose, and hemicellulose. Lignin fraction, which is only aromatic in nature, normally consists of 20–40 wt.% dry biomass [63]. Scheme 2 shows the proposed mechanism for tar formation assuming lignin units as precursors. The

three lignin-units of vanillin ($C_8H_8O_3$), guaiacol ($C_7H_8O_2$), and catechol ($C_6H_6O_2$) are pyrolyzed or react with hydrogen. The reaction pathway was chosen according to the most thermodynamically favorable reactions. Reaction R1 represents the vanillin pyrolysis, and reaction R1a is the vanillin reacting with hydrogen. Phenol is transformed into cyclopentadiene, and CO is abstracted from the phenol according to reaction R4. Afterward, cyclopentadiene combines to form naphthalene in accordance with reaction R7 [63,64].
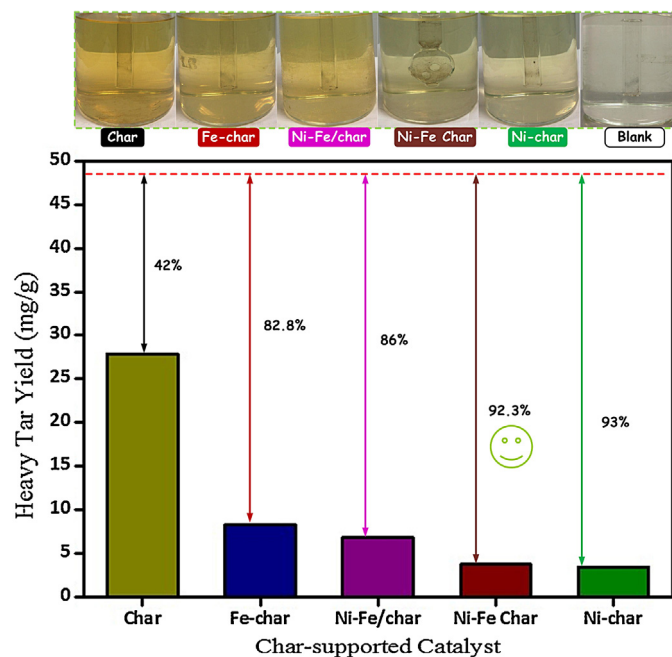

Fig. 6. Heavy tar yield and conversion efficiency with char and different char-supported catalysts.
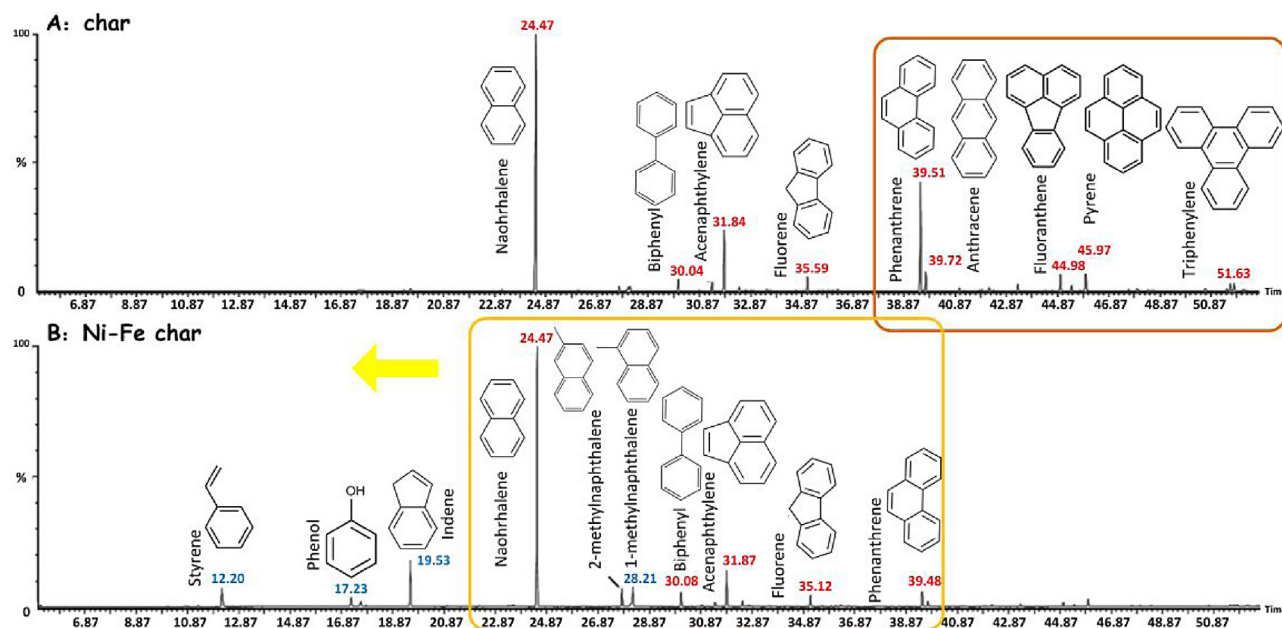
Fig. 7. Light tar composition during RH pyrolysis with char and Ni–Fe char catalyst.

Fig. 6 shows the condensable tar (heavy tar) yield and conversion efficiency with different char-supported catalysts. From the tar instance graphs after *in-situ* reforming, it can intuitively be observed that the tar yield for RH pyrolysis was decreased by mixing with the char-supported catalysts. The biomass tar removal efficiency was only 42% mixed with pyrolysis char; whereas it can reach about 93% mixed with Ni-char catalyst. It indicates that Ni-based catalysts indeed have higher tar cracking and reforming performances as reported in the ref. [65]. The metallic Ni catalyst exhibited much higher reforming activity of hydrocarbons than metallic Fe catalysts caused by the high activation ability of C—H and C—C bond in the hydrocarbon molecules on the Ni metal surface. Compared with the two bimetallic catalysts (Ni-Fe/char, Ni-Fe char), the Ni-Fe char without calcination shows a higher tar removal efficiency (92.3% *vs.* 86%). According the catalysts characterization, the Ni-Fe/char is mainly in form of SiO_2-supported catalyst (RHA/Ni-Fe), whereas the Ni-Fe char is the C-SiO_2 supported catalyst (RH char/Ni-Fe). Carbon in the Ni-Fe char plays a significant role for tar reforming. On one hand, porous carbon can enhance the BET surface area of catalysts contributing to the sorption effect; one the other hand, carbon itself can work as a medium decreasing metal oxides and tar at high temperature by reductive reactions. Guan et al. [66] proposed that parts of metal oxides can be reduced into a metallic state by the syngas (H_2 and CO) initially produced from the biomass pyrolysis without the aid of the catalyst. Therefore, Fe and Ni in their metallic forms rather than their oxide forms were considered the active sites for the tar reforming. Besides, it is possible that Ni^{2+} in the Ni-Fe char catalyst can be easier reduced into metallic state of Ni (Ni^0) than NiO in the Ni-Fe/char catalyst. Consideration of convenience and economical efficiency, the bimetallic Ni-Fe char catalyst without calcinations and H_2-pretreatment could be employed for tar conversion. The synergy effect between the activation of tar on the Ni species and the oxygen atom supplied to the carbonaceous intermediate from neighboring Fe atoms was not displayed. Probably without the presence of steam or water, the Fe distribution in the samples after pyrolysis shows an imbalance between the phases FeO and Fe_3O_4 providing for tar reforming. Those Fe species always take place in the redox equations of the water gas shift (WGS) reactions (1) and (2). Thus, the steam reforming with the char-supported monometallic Fe and bimetallic Ni-Fe

catalysts should be further studied in order to enhance the tar conversion efficiency and H_2 yield.

$$Fe_3O_4 + CO \leftrightarrow 3FeO + CO_2 \qquad (1)$$

$$3FeO + H_2O \leftrightarrow H_2 + Fe_3O_4 \qquad (2)$$

As shown in Fig. 7, the tar composition from RH pyrolysis is dominated by polycyclic aromatic compounds, such as indene, naphthalene, methylnaphthalenes, biphenyl, acenaphthylene, fluorine and phenanthrene. These aromatic species have been considered as tar compounds in different thermal processes such as pyrolysis and gasification of both biomass and wastes. Although benzene and toluene have been also reported as tar compounds, they are volatile enough to be lost during the collection and analyzing process. Herein, the resulting samples were deficient in lighter compounds such as benzene. By using the Ni-Fe char catalyst, the signals of 3 and 4-ring compounds were reduced and cracked into 2-ring or 1-ring compounds, such as phenanthrene; however, single-ring compounds such as styrene are detected in the chromatograms. The lighter hydrocarbons can be subsequently aromatized via Diels–Alder type reactions due to the thermal degradation of alkanes into alkenes resulting in the formation of single-ring compounds such as toluene and styrene. The following reactions show the possible formation mechanism for toluene
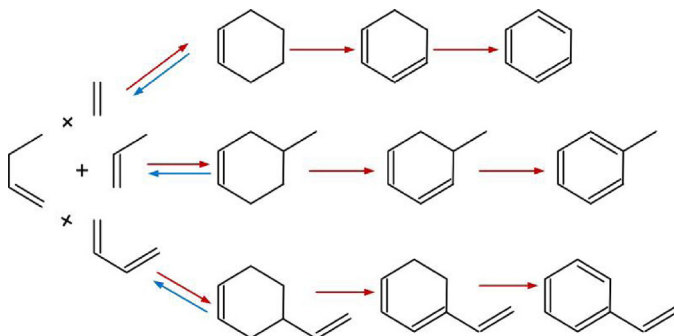
Scheme 3. The formation mechanism for toluene and alkylaromatics produced by thermal degradation of alkanes via Diels–Alder reaction.
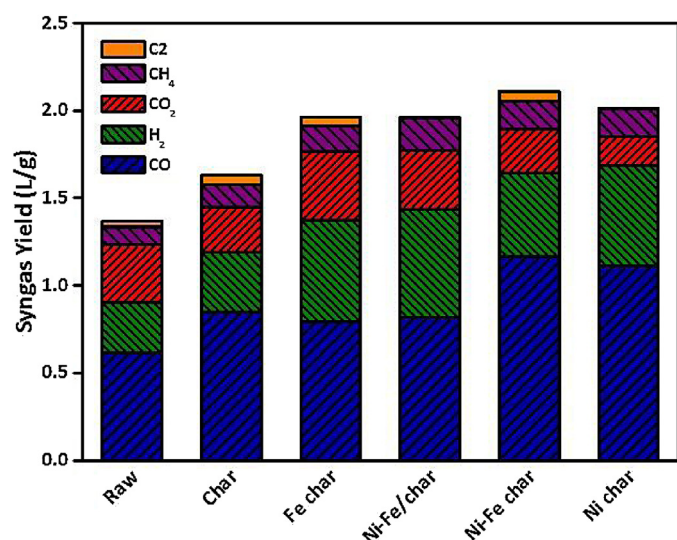
Fig. 8. Gas yield and composition with char and different char-supported catalyst.

Table 3
The LHV of the gaseous products using different RH char-supported catalysts.

Catalyst type	No catalyst	Char	Fe char	Ni–Fe/char	Ni–Fe char	Ni char
LHV (MJ/m^3)	10.64	11.69	10.95	11.93	12.10	12.80

and alkylaromatics produced by alkanes thermal-degradation via Diels–Alder reaction (Scheme 3).

3.4. Gas yield and composition

Synthesis gas is the prime product of biomass pyrolysis. Their properties can reflect the pyrolysis and tar reforming efficiency with different catalysts, because tar is cracked and converted into small molecules gases by catalytic thermochemical reforming. The gas yield could be estimated by Eq. (1). In addition, the concentration of main syngas composition (i.e., H_2, CO, CO_2, CH_4, C_2H_4 and C_2H_6) can be calculated by Eqs. (2)–(6).

$$\text{Gas yield (L/g)} = \frac{\text{exit gas (L)} - N_2\text{flow rate (L/ min)} \times \text{pyrolysis time (min)}}{\text{feedstock weight (g)}} \quad (1)$$

$$H_2\,(vol.\%) = \frac{H_2\,(\%)}{H_2\,(\%) + CO\,(\%) + CO_2\,(\%) + CH_4\,(\%) + C_2H_4\,(\%) + C_2H_6\,(\%)} \quad (2)$$

$$CO\,(vol.\%) = \frac{CO\,(\%)}{H_2\,(\%) + CO\,(\%) + CO_2\,(\%) + CH_4\,(\%) + C_2H_4\,(\%) + C_2H_6\,(\%)} \quad (3)$$

$$CO_2\,(vol.\%) = \frac{CO_2\,(\%)}{H_2\,(\%) + CO\,(\%) + CO_2\,(\%) + CH_4\,(\%) + C_2H_4\,(\%) + C_2H_6\,(\%)} \quad (4)$$

$$CH_4\,(vol.\%) = \frac{CH_4\,(\%)}{H_2\,(\%) + CO\,(\%) + CO_2\,(\%) + CH_4\,(\%) + C_2H_4\,(\%) + C_2H_6\,(\%)} \quad (5)$$

$$C_2\,(vol.\%) = \frac{C_2H_4\,(\%) + C_2H_6\,(\%)}{H_2\,(\%) + CO\,(\%) + CO_2\,(\%) + CH_4\,(\%) + C_2H_4\,(\%) + C_2H_6\,(\%)} \quad (6)$$

Fig. 8 shows the gas yield and syngas composition when different catalysts were used. It can be seen that the total gas yield increased when the char and char-supported catalysts were used, almost corresponding to the results of tar reforming efficiency. The increase of gas yield may be attributed to the thermochemical reactions between char, tar and catalysts at higher temperature. On one hand, char can react with syngas (i.e., CO_2 and H_2) to produce more other gas components (i.e., CO, CH_4); on the other hand, tar can be cracked into gas components by dry reforming over char and char-supported catalysts. In particular, the gas yield can approximately reach 2.11 L/g when fast pyrolysis of RH and Ni–Fe char mixture at 800 °C. When char was mixed with RH, the CO volume concentration increased from 44.8% to 52.0%, whereas, the CO_2 volume concentration decreased from 24.0% to 15.8%. It suggested that CO_2 reacted with char (C) resulting in the increase of CO volume concentration. Meanwhile, the methane (CH_4) volume concentration could increase from 7.5% to 8.0% possibly attributed to the methanation reactions between CO_2, C and H_2. Thus, char itself could be used as an adsorbent and catalyst for tar reforming and CO_2 conversion.

Because of char *in-situ* sorption enhanced and co-catalyst effect, Ni–Fe char catalyst could obtain a higher gas yield than Ni–Fe/char catalyst (2.11 L/g *vs.* 1.96 L/g). From the volume concentrations of CO (55.2% *vs.* 41.8%) and H_2 (22.7% *vs.* 31.5%), it can also conclude that H_2 was, to some extent, consumed with the presence of char and metal oxides at high temperature. Although high concentration of H_2 was not obtained, CO and CH_4 volume concentration got improved. It should be noted that compared with raw yield (24.0%), CO_2 volume concentrations greatly decreased (the yields as follows: 15.8%, 11.9%, and 8.2%) by using char, Ni–Fe char and Ni char catalysts, respectively. Furthermore, it corresponds to the previous result that NiO playing a critical role in decreasing the carbon deposit and increasing the amount of CO in the gaseous product [67]. The low heating values (LHV) of the gas products are calculated from Eq. (7) [68], where (CO), (H_2), and (CH_4) are the gas volume concentration of the product gas in Fig. 8. The results are shown in Table 3. The LHV values can typically reach the range from 10.64 MJ/m^3 to 12.80 MJ/m^3 at 800 °C indicating a good quality of the syngas.

$$LHV\,(kJ/m^3) = [30\,(CO) + 25.7\,(H_2) + 85.4\,(CH_4)] \times 4.2 \quad (7)$$

3.5. XPS analysis

X-ray photoelectron spectroscopy (XPS) has been extensively used in studies of the surface chemistry of metals, alloys, oxides and hydroxides with particular reference to oxidation, corrosion and chemical attack including acid dissolution. The XPS spectra of the studied catalysts indicated the presence of four distinct peaks due to nickel, iron, silica and carbon. The XPS patterns of Ni 2p, Si 2p, and C 1s regions for the Ni char catalyst are depicted in Fig. 9A, with the curve-fitting spectra included. It is clearly observed that an understanding of multiplet splitting and satellite structure is crucial to the interpretation of the Ni 2p line-shape. >In general, charging effects were corrected by adjusting the binding energy (B.E.) of C 1s to 284.6 eV. The B.E. of NiO usually distributes at 853.3 eV in the standard spectrum. However, the Ni 2p3/2 peak of Ni char centered at 855.1 eV attributed to the strong interaction with the support (e.g., silica, alumina) indicating the presence of NiO or other substances between NiO and NiAl$_2$O$_4$ spinel. Presence of satellite peaks demonstrated nickel atoms in the forms of NiO or Ni$_2$O$_3$ were present in oxygen environment for calcination. After reaction, the satellite peaks disappeared possibly because of carbon thermal reduction under the oxygen-free condition (N$_2$ atmosphere), which was in accord with the results of XRD analysis. Meanwhile, more disordered small peaks appeared around 852.0 eV indicating the peaks of metallic Ni possibly due to nickel oxides reduction (Fig. 9B). It was reported that nickel oxide shows little interaction with silica but strong interaction with alumina in the impregnated catalysts after calcination. NiO can react with Al$_2$O$_3$ in air at 450–600 °C to generate NiAl$_2$O$_4$ spinel on the surface [69]. NiAl$_2$O$_4$ at the B.E. of 855.4 eV is present in the Ni-char catalyst (Fig. 9). The spinel peak was not detected by XRD measurement explained by the poor crystallinity and trace amount of spinel produced at the lower calcination temperature and the shorter calcination time. Besides, it can be obviously seen that the C energy loss peak at around 296 eV in Ni char catalyst, indicating that carbon in RH char became more stable after reaction.

Although oxidizing gases may be generated from nitrate salt decomposition, the only crystalline species observed are reduced
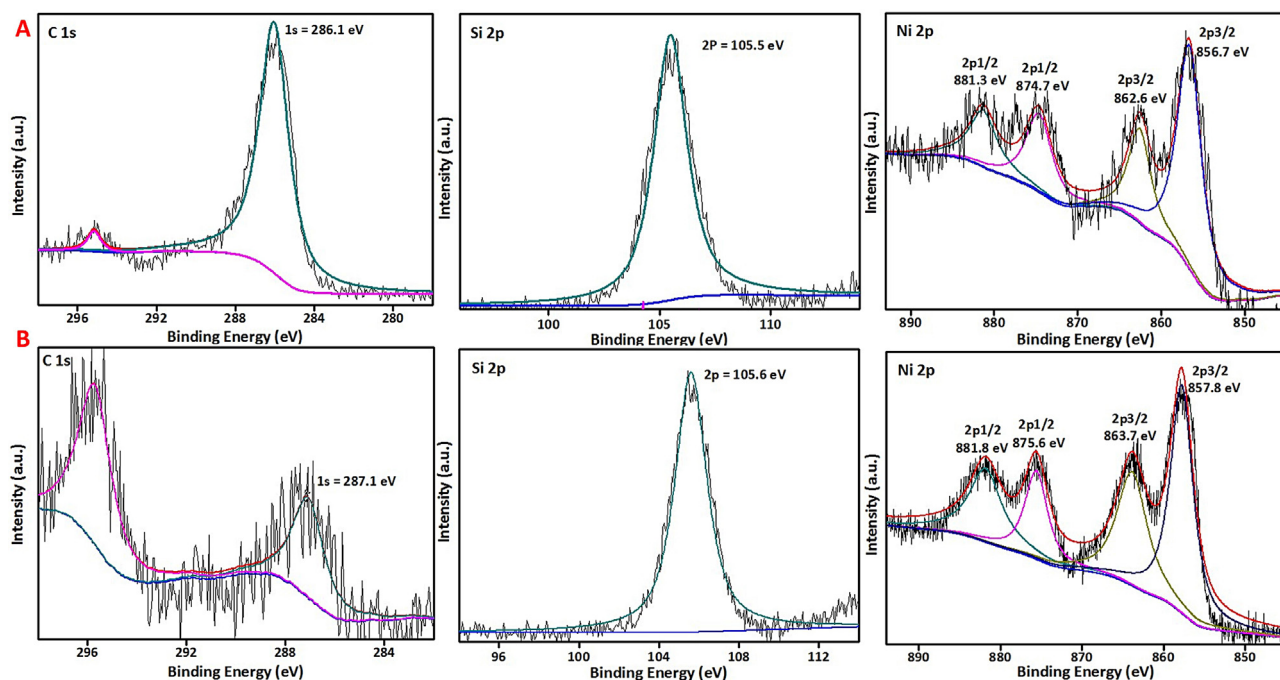
Fig. 9. XPS patterns of Ni char catalyst before and after reaction.

iron oxides, suggesting that the impact of these low concentration gases on the chemical impregnated iron oxides is negligible. It was reported that Fe_2O_3 could be reduced into Fe_3O_4 or other reduced iron species by CO and H_2 (synthesis gas from biomass pyrolysis) [70]. The peak positions of Fe 2p1/2 and Fe 2p3/2 depend on the ionic states of Fe. Meanwhile, the satellite peak positions for the Fe 2p1/2 and Fe 2p3/2 peaks are very sensitive to the oxidation states. Thus, these peaks could be used for qualitatively determining the ionic states of iron. Commonly, the B.E.s of FeO, Fe_3O_4, Fe_2O_3 and FeO(OH) distribute, respectively, at 109.4, (708.2, 710.4), 710.9 and 711.3 eV in the standard spectrum. The XPS patterns of Ni 2p, Fe 2p, Si 2p, and C 1s regions for the fresh Ni–Fe char catalyst are depicted in Fig. 10A. Of the two peaks of Fe 2p, Fe 2p3/2 peak is narrower and stronger than Fe 2p1/2 and the area of Fe 2p3/2 peak is greater than that of Fe 2p1/2 because in spin-orbit (j–j) coupling; Fe 2p3/2 has degeneracy of four states whilst Fe 2p1/2 has only two [71]. The fresh Ni–Fe char catalyst showed that the Ni 2p3/2 B.E. at 856.7 eV

identified as the peak of $Ni(OH)_2$, and the Fe 2p3/2 B.E. at 711.1 eV identified as the peak of FeO(OH) or other substances between Fe_2O_3 and FeO(OH). The Fe 2p3/2 peak also has associated satellite peaks indicating the presence of Fe^{2+} and Fe^{3+}, which is located approximately 8 eV higher than the main Fe 2p3/2 peak (Fig. 10A). Indeed, Fe_2O_3 and Fe_3O_4 existed in the fresh Ni–Fe char catalyst, in agreement with the XRD data. After reaction (Fig. 10B), all the peaks of Fe 2p3/2, Fe 2p1/2, Ni 2p3/2 and Ni 2p1/2 shifted substantially to the left. The reason can be ascribed to the enhancement of carbon adsorption due to structure change of carbon-based material. Without calcination, the carbon loss peak cannot be observed in the Ni–Fe char catalyst. Moreover, the C 1s peak was divided attributed to the presence of other organic functional groups (i.e., C=O, C—H, C—C, C—OH, COOH), which may be ascribed to tar deposit on the char surface. Besides, it can be observed that metallic state of Ni (Ni^0) *in-situ* generated in the Ni–Fe char catalyst after reaction, characterized by the Ni 2p3/2 peak at around 852.7 eV. Thus, the
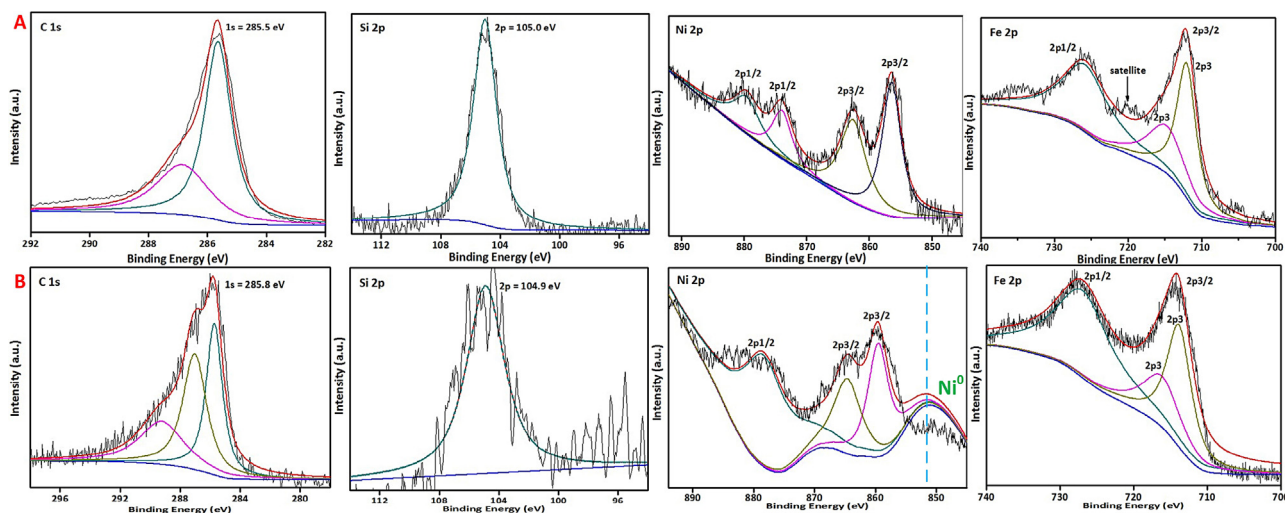

Fig. 10. XPS patterns of Ni–Fe char catalyst before and after reaction.
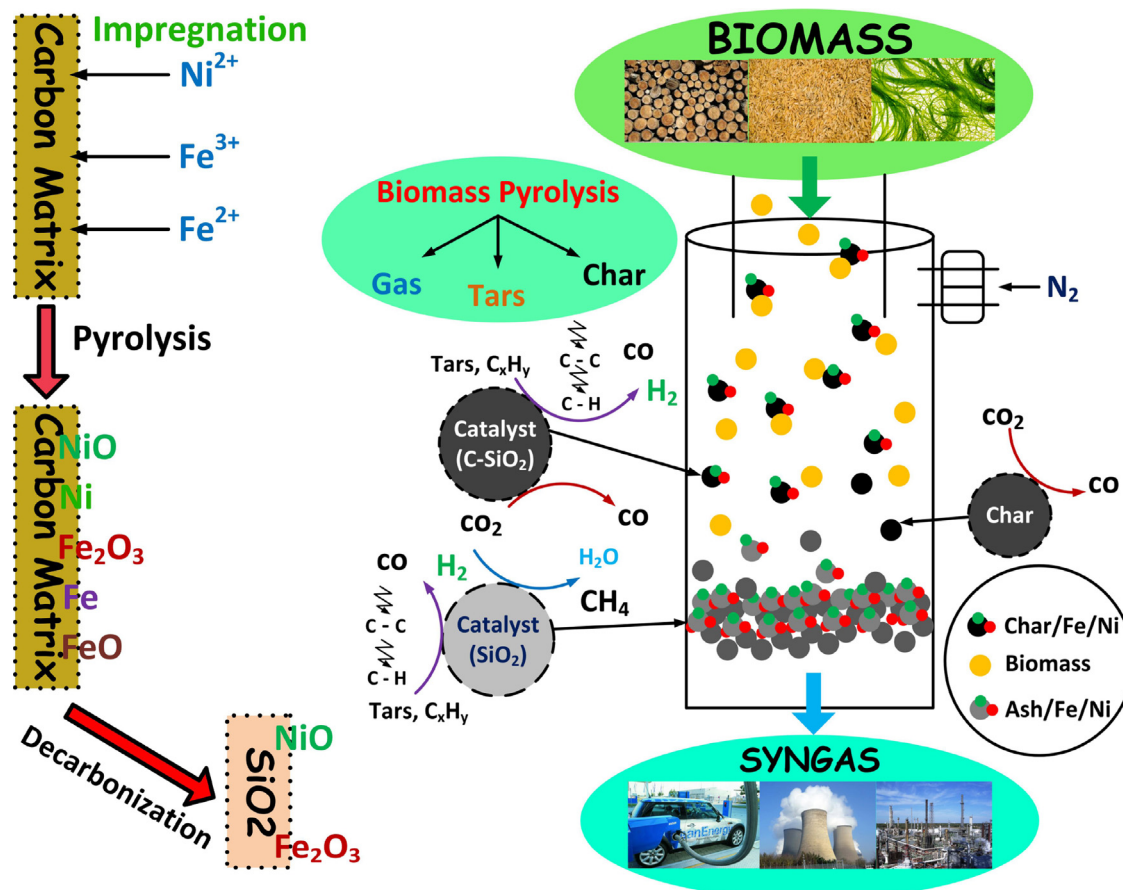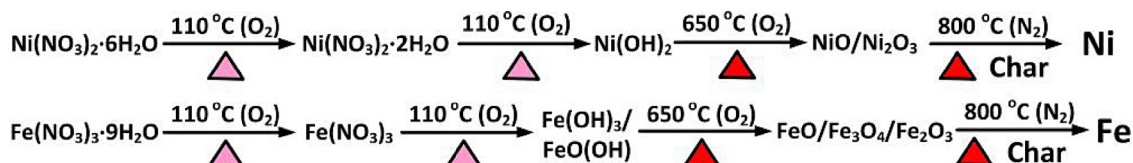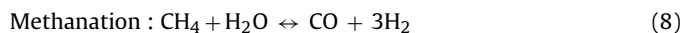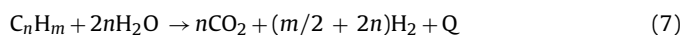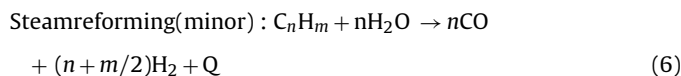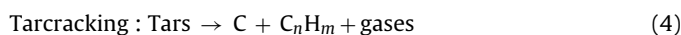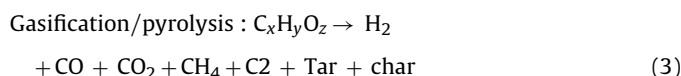
Fig. 11. Mechanism of *in-situ* tar conversion for biomass pyrolysis using RH char-supported Ni–Fe catalysts.

chemical state changes of the char-supported Ni–Fe char catalyst can be summarized as Scheme 4.
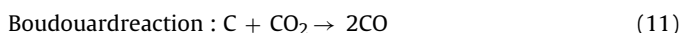
3.6. Tar catalytic conversion mechanisms

The potential mechanisms of biomass gasification and tar reforming could be expressed by the partial combustion reactions, heterogenous reactions and homogenous reactions (3)–(14). Catalytic reforming reactions cleave the C—C and C—H bonds of the carbohydrate backbone to yield a combination of CO and H_2 (reactions (5)–(7)) [72]. If water (H_2O) is in presence, CO_2 can be formed via the WGS reaction to produce more H_2 (reaction (14)). Aqueous-phase reforming (APR) using bimetallic catalysts can produce H_2 and CO_2 starting with sugars and sugar alcohols [73]. The selectivity towards hydrogen can be controlled using catalysts with different metal composites (e.g., Pt) and metal–alloys (e.g., Raney Ni–Sn) [74]. Abu El-Rub [48] thought that tars can be adsorbed on the active sites of char particles. The adsorbed tars and cokes can be catalytically reformed to CO and H_2 by steam and dry thermochemical reactions. Meanwhile, free radicals that enter polymerization reactions and coke on char surfaces can be formed from tar decomposition. The gasification reactions of coke cannot only increase CO and H_2 in
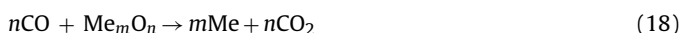
syngas, but also refresh the active surface area of char at temperature above 800 °C [48]. These reactions may explain the increasing trend of CO followed by temperature because more CO than H_2 is produced. As char is utilized as a catalyst support, char may react with CO_2 to produce the extra CO and CH_4 without additional steam and oxygenated compounds (reactions (8) and (9)).

$$\text{Gasification/pyrolysis}: C_xH_yO_z \rightarrow H_2$$
$$+ CO + CO_2 + CH_4 + C2 + Tar + char \tag{3}$$

$$\text{Tar cracking}: Tars \rightarrow C + C_nH_m + gases \tag{4}$$

$$\text{Dry reforming (major)}: C_nH_m + nCO_2 \rightarrow 2nCO + (m/2)H_2 + Q \tag{5}$$

$$\text{Steam reforming (minor)}: C_nH_m + nH_2O \rightarrow nCO$$
$$+ (n + m/2)H_2 + Q \tag{6}$$

$$C_nH_m + 2nH_2O \rightarrow nCO_2 + (m/2 + 2n)H_2 + Q \tag{7}$$

$$\text{Methanation}: CH_4 + H_2O \leftrightarrow CO + 3H_2 \tag{8}$$

Scheme 4. Chemical state changes of char-supported Ni–Fe catalysts.

$$CO_2 + 4H_2 \leftrightarrow CH_4 + 2H_2O \tag{9}$$

$$C + 2H_2 \leftrightarrow CH_4 \tag{10}$$

$$\text{Boudouard reaction}: C + CO_2 \rightarrow 2CO \tag{11}$$

Water gas reaction: char (C) may react with water for additional hydrogen generation.

$$C + H_2O \rightarrow CO + H_2 \tag{12}$$

$$C + 2H_2O \rightarrow CO_2 + 2H_2 \tag{13}$$

$$WGS: CO + H_2O \rightarrow CO_2 + H_2 \tag{14}$$

$$\text{Carbon } in\text{-}situ \text{ reduction (major)}: C + Me^{2+} \rightarrow Me + C^{2+} \tag{15}$$

$$nC + Me_mO_n \rightarrow mMe + nCO \tag{16}$$

$$\text{Gas } in\text{-}situ \text{ reduction (minor)}: nH_2 + Me_mO_n \rightarrow mMe + nH_2O \tag{17}$$

$$nCO + Me_mO_n \rightarrow mMe + nCO_2 \tag{18}$$
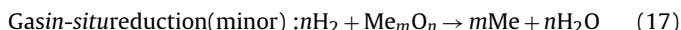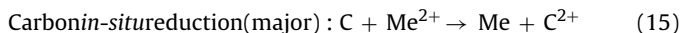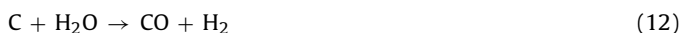
Note: Me^{2+} and Me_mO_n refer to metal ions and metallic oxides, respectively.

In this work, monometallic Ni catalysts exhibited much higher reforming activity of hydrocarbons than monometallic Fe catalysts. This property is caused by the high activation ability of C—H and C—C bond in the hydrocarbon molecules on the Ni metal surface. Consequently, it seems that the additive effect of Fe is the increase of the number of active Ni surface, but the characterization results on the particle size and surface enrichment of Fe on the Ni–Fe bimetallic particles did not support the increase of the surface Ni atoms. Another possibility is that Fe has co-catalytic function. Since Fe has high oxygen affinity than Ni, the addition of Fe to Ni catalysts can increase the coverage of oxygen atoms during the reforming reactions. The catalytic activity of Ni–Fe catalysts for tar elimination can be concluded in the following order: Ni-char > Ni–Fe char > Ni–Fe/char > Fe-char > char. To some extent, carbon and gas *in-situ* reduction could occur in char, reducing gas and metal oxides or ions during biomass pyrolysis, which transformed partial metal oxides or ions into metallic states (reactions (15)–(18)) contributing to the enhancement of tar conversion.

Fig. 11 can summarize the tar *in-situ* conversion mechanism over the RH char-supported Ni–Fe catalysts. In the pyrolyzer, biomass was initially cracked into the gas, tar and char by thermochemical reactions. The produced tar can be cracked and reformed simultaneously over the RH char-supported Ni–Fe catalysts under high temperature. After that, parts of RH char-supported catalysts (C–SiO$_2$ catalysts) could be converted into SiO$_2$-based catalysts because of high-content nano-sized amorphous SiO$_2$ in RH char. In summary, RH char plays two significant roles during the process of biomass pyrolysis. On one hand, it works as an intermediate reductant to reduce the metal oxides and CO$_2$; on the other hand, it can be considered as an adsorptive-support to adsorb metal ions and tar. To our knowledge, the sublimation temperatures of Ni and Fe can reach up to 2732.0 °C and 1535 °C, respectively. Therefore, the metal catalysts still remain in the pyroylsis char in the form of solid states, which could be regenerated via thermal regeneration using waste heat or gasified into syngas directly.

4. Conclusions

An alternative biomass catalytic pyrolysis/gasification technology with *in-situ* tar conversion has been developed. Mixing with the RH char and char-supported Ni–Fe catalysts, the tar yield and CO$_2$ concentration during biomass pyrolysis were greatly decreased, especially in terms of 92.3% of the heavy tar removal efficiency by the Ni-Fe char. Using the Ni-Fe char catalyst, the light tar with 3 and 4-ring organic compounds could were reduced and cracked into single ring compounds or syngas. It is worth pointing out

that partial metal oxides via carbon and gas *in-situ* reduction were transformed into metallic states enhancing the catalytic performance, especially in terms of tar conversion. Meanwhile, a higher gas yield of 2.11 L/g was obtained by adding the Ni-Fe char catalyst attributed to char *in-situ* sorption enhanced and co-catalyst effect. Although the bimetallic Ni-Fe char-supported catalysts (Ni-Fe/char, Ni-Fe char) exhibited lower tar reforming efficiency compared with the monometallic Ni char catalyst, the synthesis expense was cheaper because of low-concentration Ni used. Moreover, omitting the step of calcination, the preparation procedure of catalysts became much simple and energy saving. Without water, the synergy effect between the activation of tar on the Ni species and the oxygen atom supplied to the carbonaceous intermediate from neighboring Fe atoms was not displayed in this dry conversion process. Thus, the bimetallic Ni-Fe char catalyst will be further studied in a pyrolysis-reforming facility (steam *vs.* dry). In our opinion, the char-supported catalysts are recommended for low-oxygen biomass gasification process (e.g., pyrolysis). Reacting with oxygen at high temperature, char and char-supported catalysts could be easier consumed, possibly shorten their service life and increasing CO$_2$ concentration in syngas.

Acknowledgements

References

[1] W. Torres, S.S. Pansare, J.G. Goowin Jr., Catal. Rev. 49 (2007) 407–456.
[2] G.J. Stiegel, R.C. Maxwell, Fuel Process Technol. 71 (2001) 79–97.
[3] I.I. Ahmed, N. Nipattummakul, A.K. Gupta, Appl. Energy 88 (2011) 165–174.
[4] I.I. Ahmed, A.K. Gupta, Appl. Energy 86 (2009) 1732–1740.
[5] A.V. Bridgwater, Fuel 74 (1995) 631–653.
[6] J. Han, H. Kim, Renew. Sustain. Energy Rev. 12 (2008) 397–416.
[7] D. Mohan, C.U. Pittman, P.H. Steele, Energy Fuels 20 (2006) 848–889.
[8] C. Di Blasi, Prog. Energy Combust. Sci. 34 (2008) 47–90.
[9] D. Neves, H. Thunman, A. Matos, L. Tarelho, A.G. Barea, Prog. Energy Combust. Sci. 37 (2011) 611–630.
[10] A. Gómez-Barea, B. Leckner, Gasification of biomass and waste, in: Handbook of Combustion, vol. 5, Wiley, 2010, pp. 365–399.
[11] G.Q. Guan, G. Chen, Y. Kasai, E.W.C. Lim, X.G. Hao, M. Kaewpanha, A. Abuliti, C. Fushimi, A. Tsutsumi, Appl. Catal. B: Environ. 115–116 (2012) 159–168.
[12] P. Hasler, T. Nussbaumer, Biomass Bioenergy 16 (1999) 385–395.
[13] T. Phuphuakrat, T. Namioka, K. Yoshikawa, Appl. Energy 87 (2010) 2203–2211.
[14] A. Paethanom, S. Nakahara, M. Kobayashi, P. Prawisudha, K. Yoshikawa, Fuel Process Technol. 104 (2012) 144–154.
[15] L. Fagbemi, L. Khezami, R. Capart, Appl. Energy 69 (2001) 293–306.
[16] S.A. Nair, A.J.M. Pemen, K. Yan, E.J.M. Van Heesch, K.J. Ptasinski, A.A.H. Drinkenburg, Plasma Chem. Plasma Process. 23 (2003) 665–680.
[17] E.G. Baker, L.K. Mudge, J. Anal. Appl. Pyrol. 6 (1984) 285–297.
[18] D. Wang, W. Yuan, W. Ji, Trans. ASABE 53 (2010) 795–800.
[19] Z. Abu El-Rub, E.A. Bramer, G. Brem, Ind. Eng. Chem. Res. 43 (2004) 6911–6919.
[20] Y. Shen, K. Yoshikawa, Renew. Sustain. Energy Rev. 21 (2013) 371–392.
[21] G.W. Huber, S. Iborra, A. Corma, Chem. Rev. 106 (2006) 4044–4098.
[22] Q.Z. Yu, C. Brage, T. Nordgreen, K. Sjöström, Fuel 88 (2009) 1922–1926.
[23] B. Dou, J. Gao, X. Sha, S.W. Baek, Appl. Therm. Eng. 23 (2003) 2229–2239.
[24] S.S. Tamhankar, K. Tsuchiya, J.B. Riggs, Appl. Catal. 16 (1985) 103–121.
[25] T. Suzuki, H. Ohme, Y. Watanabe, Energy Fuels 6 (1992) 343–351.
[26] M. He, B. Xiao, Z. Hu, S. Liu, X. Guo, S. Luo, Int. J. Hydrogen Energy 34 (2009) 1342–1348.
[27] D. Li, Y. Nakagawa, K. Tomishige, Chin. J. Catal. 33 (2012) 583–594.
[28] T. Furusawa, A. Tsutsumi, Appl. Catal. A: Gen. 278 (2005) 207–212.
[29] S.J. Juutilainen, P.A. Simell, A.O. Krause, Zirconia, Appl. Catal. B: Environ. 1-2 (2006) 86–92.
[30] D.A. Constantinou, M.C. Álvarez-Galván, J.L.G. Fierro, A.M. Efstathiou, Appl. Catal. B: Environ. 117–118 (2012) 81–95.
[31] S. Cheah, K.R. Gaston, Y.O. Parent, M.W. Jarvis, T.B. Vinzant, K.M. Smith, N.E. Thornburg, M.R. Nimlos, K.A. Magrini-Bair, Appl. Catal. B: Environ. 134-135 (2013) 34–45.
[32] P. Azadi, E. Afif, H. Foroughi, T. Dai, F. Azadi, R. Farnood, Appl. Catal. B: Environ. 134-135 (2013) 265–273.
[33] H. Zhao, K.J. Draelants, G.V. Baron, Ind. Eng. Chem. Res. 39 (2000) 3195–3201.
[34] D.N. Bangala, N. Abatzoglou, E. Chornet, AIChE J. 44 (1998) 927–936.

[35] C.M. Kinoshita, Y. Wang, J. Zhou, Ind. Eng. Chem. Res. 34 (1995) 2949–2954.
[36] J. Corella, A. Orío, J. Toledo, Energy Fuels 13 (3) (1999) 702–709.
[37] P.H. Blanco, C. Wu, J.A. Onwudili, P.T. Williams, Appl. Catal. B: Environ. 134–135 (2013) 238–250.
[38] C. Li, D. Hirabayashi, K. Suzuki, Appl. Catal. B: Environ. 3–4 (2009) 351–360.
[39] T. Kimura, T. Miyazawa, J. Nishikawa, S. Kado, K. Okumura, T. Miyao, S. Naito, K. Kunimori, K. Tomishige, Appl. Catal. B: Environ. 3–4 (2006) 160–170.
[40] F. Pompeo, N.N. Nichio, O.A. Ferretti, D. Resasco, Int. J. Hydrogen Energy 30 (2005) 1399–1405.
[41] V.R. Choudhary, A.S. Mamman, Appl. Energy 66 (2000) 161–175.
[42] T.J. Wang, J. Chang, C.Z. Wu, Y. Fu, Y. Chen, Biomass Bioenergy 28 (2005) 508–514.
[43] C. Courson, L. Udron, D.W. Ski, C. Petit, A. Kiennemann, Catal. Today 76 (2002) 75–86.
[44] I.G. Lee, S.K. Ihm, Ind. Eng. Chem. Res. 48 (2009) 1435–1442.
[45] D.D. Le, X. Xiao, K. Morishita, T. Takarada, J. Chem. Eng. Jpn. 42 (2009) 51–57.
[46] Z. Abu El-Rub, E.A. Bramer, G. Brem, Fuel 87 (2008) 2243–2252.
[47] Z. Abu El-Rub, E.A. Bramer, G. Brem, Tar reduction in biomass gasification using biomass char as a catalyst, in: Proceeding of Conference and Technology Exhibition on Biomass for Energy, Industry and Climate Protection, Rome, Italy, 2004, pp. 1046–1049.
[48] Z. Abu El-Rub, Biomass Char as an *in-situ* Catalyst for Tar Removal in Gasification Systems, University of Twente, Enschede, 2008 (Ph.D. Dissertation).
[49] P. Gilbert, C. Ryu, V. Sharific, J. Swithenbank, Bioresource Technol. 100 (2009) 6045–6051.
[50] C. Danny, K. Ko, J.F. Porter, G. McKay, Chem. Eng. Sci. 55 (1999) 5819–5829.
[51] D. Wang, W.Q. Yuan, W. Ji, Appl. Energy 88 (2011) 1656–1663.
[52] V. Nemanova, T. Nordgreen, K. Engvall, K. Sjöeströem, Catal. Today 176 (2011) 253–257.
[53] H.B. Liu, T.H. Chen, X.L. Zhang, J.H. Li, D.Y. Chang, L. Song, Chin. J. Catal. 31 (2010) 409–414.
[54] M. Virginie, C. Courson, D. Niznasky, N. Chaoui, A. Kiennemann, Appl. Catal. B: Environ. 101 (2010) 90–100.
[55] L. Wang, Y. Hisada, M. Koike, D. Li, H. Watanabe, Y. Nakagawa, K. Tomishige, Appl. Catal. B: Environ. 121–122 (2012) 95–104.
[56] J. Fermoso, F. Rubiera, D. Chen, Energy Environ. Sci. 5 (2012) 6358–6367.
[57] S.V.B. van Paasen, Guideline for sampling and analysis of tar and particles in biomass producer gas, ECN-C-02-090, November 2002.
[58] Y. Chen, Y.C. Zhu, Z.C. Wang, Y. Li, L.L. Wang, L.L. Ding, et al., Adv. Colloid Interface Sci. 163 (2011) 39–52.
[59] A. Karera, S. Nargis, S. Patel, M. Patel, J. Sci. Ind. Res. 45 (1986) 441.
[60] S. Chandrasekhar, P.N. Pramada, Adsorption 12 (2006) 27–43.
[61] A. Paethanom, K. Yoshikawa, Energies 5 (2012) 4941–4951.
[62] Y.D. Yeboah, J.P. Longwell, J.B. Howard, W.A. Peters, Ind. Eng. Chem. Process Des. Dev. 19 (1980) 646–653.
[63] C. Palma Font, Energy Fuels 27 (2013) 2693–2702.
[64] C. Palma Font, Appl. Energy 111 (2013) 129–141.
[65] C. Wu, P.T. Williams, Biofuels 2 (4) (2011) 451–464.
[66] G. Guan, G. Chen, Y. Kasai, E.W.C. Lim, X. Hao, M. Kaewpanha, A. Abuliti, C. Fushimi, A. Tsutsumi, Appl. Catal. B: Environ. 115–116 (2012) 159–168.
[67] H. Liu, T. Chen, D. Chang, D. Chen, H. He, R.L. Frost, J. Mol. Catal. A: Chem. 363–364 (2012) 304–310.
[68] H.P. Kuo, S.M. Pan, H.T. Hsu, Biomass Bioenergy 35 (2011) 3025–3031.
[69] F. Chang, M. Kuo, M. Tsay, M. Hsieh, Appl. Catal. A: Gen. 247 (2003) 309–320.
[70] J.D. Atkinson, M.E. Fortunato, S.A. Dastgheib, M. Rostam-Abadi, M.J. Rood, K.S. Suslick, Carbon 49 (2011) 587–598.
[71] T. Yamashita, P. Hayes, Appl. Surf. Sci. 254 (2008) 2441–2449.
[72] E.L. Kunkes, D.A. Simonetti, R.M. West, J.C. Serrano-Ruiz, C.A. Gärtner, J.A. Dumesic, Science 322 (2008) 417–421.
[73] R. Cortright, R. Davda, J. Dumesic, Nature 418 (2002) 964–967.
[74] G.W. Huber, J. Shabaker, J. Dumesic, Science 300 (2003) 2075–2077.